Hiroyuki Ikemoto* and Takafumi Miyanaga

Structure study of the chalcogens and chalcogenides by X-ray absorption fine structure

https://doi.org/10.1515/zpc-2020-1627
Received January 27, 2020; accepted March 22, 2020

Abstract: In this review, we make a survey of the structure studies for the chalcogen elements and several chalcogenides in liquid, amorphous and nanosized state by using X-ray absorption fine structure (XAFS). The chalcogen elements have hierarchic structures; the chain structure constructed with the strong covalent bond as a primary structure, and the weaker interaction between chains as a secondary one. Existence of these two kinds of interactions induces exotic behaviors in the liquid, amorphous and nanosized state of the chalcogen and chalcogenides. XAFS is a powerful structure analysis technique for multi-element systems and the disordered materials, so it is suitable for the study of such as liquid, amorphous and nanosized mixtures. In section 2, the structures for the liquid state are discussed, which show the interesting semiconductor-metal transition depending on their temperatures and components. In section 3, the structure for the amorphous states are discussed. Especially, some of chalcogens and chalcogenides present the photostructural change, which is important industrial application. In section 4, the structures of nanosized state, nanoparticles and isolated chain confined into the narrow channel, are discussed. The studies of the nanoparticle and the isolated chain reveal the alternative role between the intrachain covalent bonds and the interchain interaction.

Keywords: chalcogen; chalcogenide; hierarchic structure; XAFS.

Dedicated to Hirohisa Endo on the occasion of his 90th birthday.

1 Introduction

Chalcogen elements (sulfur, selenium, tellurium) construct a hierarchic structure. They form ring/chain molecules with a two-fold covalent bond, and the molecules

***Corresponding author: Hiroyuki Ikemoto**, Department of Physics, University of Toyama, Toyama 930-8555, Japan, E-mail: ikemoto@sci.u-toyama.ac.jp
Takafumi Miyanaga: Department of Mathematics and Physics, Hirosaki University, Hirosaki, Aomori, 036-8561, Japan

form a stable crystal by adhering to each other in an orthorhombic S and trigonal Se and Te (t-Se and t-Te) manner. The hierarchic nature is brought about by the electronic structure of the outermost electrons s^2p^4. The energy level of the s-electrons is sufficiently lower than that of the p-electrons, so they do only slightly contribute to the bonding within the molecules. Two p-electrons form the individual covalent bonds, and the other two ones form the lone-pair (LP) orbitals in pairs. The LP band occupies the top of the valence band, and the anti-bonding band forms the bottom of the conduction band. The values of the optical gap are 2.2 and 0.33 eV for t-Se and t-Te, respectively, so they are semiconductors.

LP orbitals do not contribute to the covalent bonds directly, but they affect the conformation of the molecules. The exchange repulsion between the LP orbitals brings about a rotational barrier around the covalent bond within the molecules. Unlike for the intrachain interaction, LP orbitals play the key role for the interchain interaction. They overlap with the empty anti-bonding orbitals on adjacent chain, which induces the interchain interaction.

The covalent bond length r and the interchain's first nearest neighbor (1NN) atomic distance R of t-Se are 2.37 and 3.44 Å [1], and those of t-Te are 2.84 and 3.49 Å [2], respectively. The values of R are smaller than twice the van der Waals radius in both t-Se and t-Te [3]. This means that the interchain interaction of t-Se and t-Te is stronger than the van der Waals force. The values of the ratio R/r, which measure the strength of the interchain interaction, are 1.45 and 1.23 for t-Se and t-Te, respectively. These values imply that the interchain interaction of t-Te is stronger than that of t-Se. Se and Te atoms form a continuous series of mixtures consisting of mixed chains. Therefore, in Se-Te mixtures, the interchain interaction increases and the optical gap becomes small with increasing Te concentration.

While t-Se and t-Te are both semiconductors and have a two-fold helical chain structure, they show opposite behaviors on melting. Liquid Se (l-Se) retains its semiconductive properties [4–8] and holds its two-fold chain structure [9–11]. However, l-Te transforms to metal [5, 12]. The estimated coordination number corresponding to the nearest neighbor was approximately 3, following the neutron and X-ray diffractions [13, 14]. Therefore, it was previously assumed that l-Te has an arsenic-like three-fold coordinated network structure, which induces its metallic nature [15]. Later, the idea that l-Te has a two-fold chain structure similar to l-Se was proposed [16]. It is supported by the measurements of the neutron and X-ray diffractions with the extension of the upper limit of a static structure factor and its supercooled state [18–20]. It is interesting that the semiconductor-metal (SC-M) transition accompanies the volume contraction [21].

Although l-Se is the semiconductor with the covalent bonding at moderate temperatures and pressures, it exhibits an SC-M transition at high temperature near the vicinity of the critical point [5–8]. X-ray diffraction shows that the

coordination number of 1NN remain about two and decreases a bit with increasing temperature [11, 22]. This means that the two-fold coordinated structure remains even in the metallic region. The atomic distance of 1NN barely changes and decreases with increasing temperature. The volume contraction occurs with SC-M transition like as l-Te [23].

L-Se-Te mixtures also exhibit an SC-M transition with increasing temperature, pressure, and Te concentration [7, 8, 12, 24–26]. It is characteristic that the SC-M transition of liquid chalcogen accompanies the volume contraction against an increase in temperature [27–29]. The change of the structure was investigated by the diffraction measurements [18, 30]. As Se and Te atoms form a continuous series of mixtures, the Se and Te atoms also form chalcogenide materials with other group elements, such as, Ge-Se/Te and As-Se/Te. As is the case with l-Se-Te mixtures, the liquid chalcogenides show an SC-M transition [31–35]. The chalcogenide materials easily become glasses, which have network structures with the covalent bonds. The chalcogen and chalcogenide glasses show reversible photostructural change [36–41]. Illumination above the optical gap induces a shift in the optical gap and structural change, and the subsequent annealing recovers to the initial state, which is reversible.

The chalcogen materials have primary and secondary structures, which have different properties and strengths of interaction. It is valuable to investigate the isolated molecules, which do not interact with each other, to consider the primary structure. One approach is to confine the molecules in narrow channels or cages [42–45]. Another is to create free clusters by a supersonic jet expansion method [46–51]. The structure and properties of metal or IV-th group element nanoparticles have been intensively studied. A hierarchic structure is a contrastive one made up of metallic or IV-th group elements, where a uniform structure forms a crystal. Chalcogen nanoparticles show exotic structures and properties owing to the hierarchic structure.

X-ray absorption fine structure (XAFS) appears on the absorption edge of the X-ray absorption spectrum, and is divided into two parts: X-ray absorption near edge structure (XANES) and extended XAFS (EXAFS) [52, 53]. In EXAFS region, a single scattering process of ejected photoelectron is essential, so the formulation would be rather simple. The structure analysis procedure by EXAFS is well defined. The local structure as the interatomic distance, the coordination number and thermal or static disorder (Debye-Waller factor) around the X-ray absorbing atom can be obtained with high accuracy. On the other hand, in XANES region, the multiple scattering process is dominate and several theoretical approaches are proposed [54, 55]. The information obtained from XANES are the electronic structure and three-dimensional structure around X-ray absorbing atom.

One of the most advantage of XAFS is element selectivity by tuning the incident X-ray energy, which is quite useful for the structure analysis for multi-element systems in chalcogenide mixtures such as S, Se, Te, and also including As and Ge. An outstanding feature of the EXAFS is that there is no difference between the quality of structural parameters obtained from the crystalline and the disordered material, which makes suitable for disordered materials even in liquid state. And further, XAFS measurements are applicable under extreme measurement conditions such as high temperature and high pressure, which makes XAFS possible to study the phase transition of solid to liquid, crystalline to amorphous or glassy state, bulk to nanoparticle, and semiconductor to metal as a function of temperature or pressure.

The EXAFS function can be generally expressed by a cumulant expansion, which presents the thermal average of the local structure. Temperature dependence of the second order cumulant (which is called as Debye-Waller like factor) gives information on the thermal vibration, and that of the third order cumulant does the anharmonicity of the distribution [56]. Especially, the Debye-Waller factor is useful parameter to discuss about the strength of the bonds and the atomic interactions in the chalcogen and their mixtures.

The hierarchic structure, the intra- and inter-chain interactions, brings about the characteristic properties and structures of the chalcogens and chalcogenides in the various forms, such as, the SC-M transition accompanies by the volume contraction, the photostructural change, the structural change with the isolation and the formation of the nanoparticles. XAFS analysis is the most outstanding tool to investigate their structures, because XAFS is element selective and suitable for disordered materials. We review their structures obtained by the XAFS analysis focusing on the hierarchic structure.

2 Liquid state chalcogenides

2.1 Liquid selenium

In this section, we discuss the structure of the liquid Se comparing the solid and vapor Se. Selenium is a typical chalcogen element. The stable form of Se is trigonal, where Se atoms form the chain with the two-fold covalent bond and the chains stack each other. Liquid Se is semiconductor near the melting point as t-Se. However, l-Se shows SC-M transition at the high temperatures and pressures near the critical point, which accompanies the volume contraction. X-ray diffraction measurements show the coordination number is slightly smaller than two in the metallic region [11, 22]. The local structure of l-Se was investigated by XAFS [11, 57–62]

EXAFS spectra for l-Se are shown in Figure 1 [11]. While the EXSFS oscillations damp with increasing temperature, they are still clearly even at high temperatures. The magnitude of Fourier transform, $|FT(r)|$, of $\chi(k)$ gives us insight of interatomic correlations. Figure 2 shows the $|FT(r)|$ for t-Se, l-Se and v-Se [58]. The first peak of t-Se corresponds to the intrachain 1NN atoms, that is, the covalent bond. The second two peaks are the interchain 1NN and the intrachain second nearest neighbor atoms. In every phase, the first peaks appear clearly, but the higher order peaks reduce or disappear with increasing temperature and melting. Temperature variation shows that the two-fold covalent bond exists even in the liquid and gas phases, as is seen in the solid phase. However, the interchain interaction is weak, so it is easily reduced.

It is interesting that the covalent bond shrinks on melting, specifically, from 2.36 Å in t-Se to 2.34 Å in l-Se, while the molar volume expands [58]. This is a

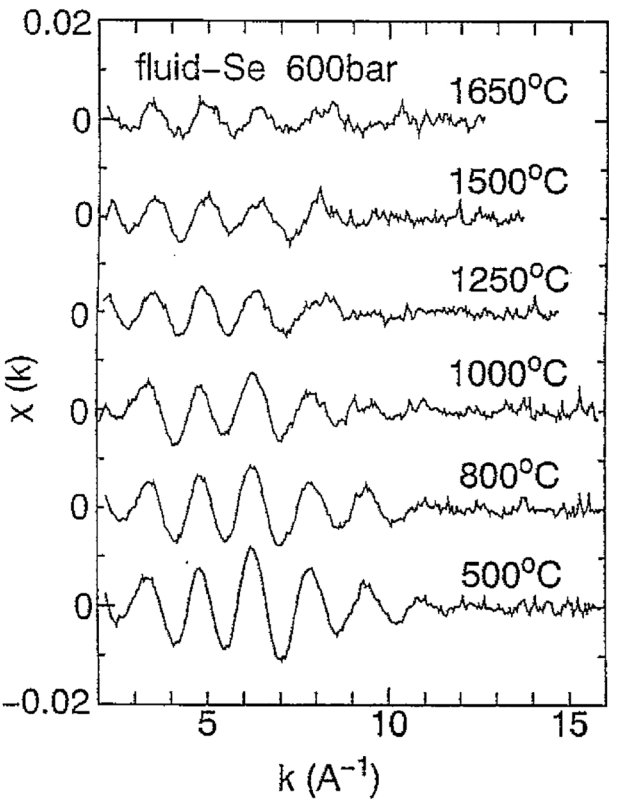

Figure 1: XAFS spectra, $\chi(k)$, of fluid-Se. Reprinted with permission from [11].

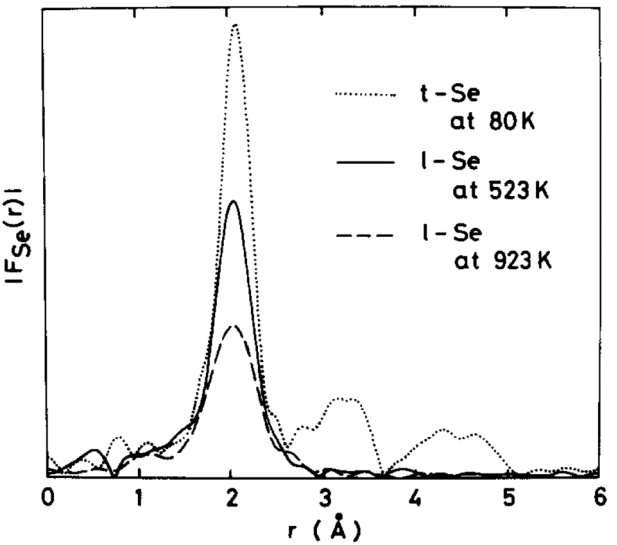

Figure 2: The magnitude of Fourier transform, $|FT(r)|$, of $\chi(k)$ of crystal, and liquid selenium. Reprinted with permission from [57].

characteristic feature of hierarchic elements, where the inter- and intra-chain interactions have different strengths and exhibit specific behaviors. On melting, the strong interchain interaction survives while the weak interchain correlation vanishes. The interchain correlation originates from the overlap between the LP orbital and the anti-bonding orbital on the adjacent chain, and weakens the covalent bond. The disappearance of the interchain interaction on melting induces strengthening and shrinkage of the covalent bond.

While l-Se is a semiconductor, it exhibits the SC-M transition at a high temperature near the critical point. A special cell and an autoclave vessel for XAFS under high temperatures and pressures enabled to obtain the XAFS spectra [11, 34]. Figure 3 shows the magnitude of $|FT(r)|$ at high temperatures, including the temperature region where the SC-M transition occurs [60]. At high temperatures, a new peak appears around 2.8 Å, which is different from any known atomic correlations in t-Se. The first peak shifts to the shorter side and becomes a broader and anisotropic peak that tails to the shorter side with increasing temperature.

A simple harmonic approximation gave unreliable values of the coordination number for the first shell. The value in the metallic state is smaller than 1, which is inconsistent with the values obtained from the diffraction data [11, 22]. Therefore, the data were analyzed with a non-harmonic analysis by using the cumulant expansion method, which gave reasonable values of the coordination numbers

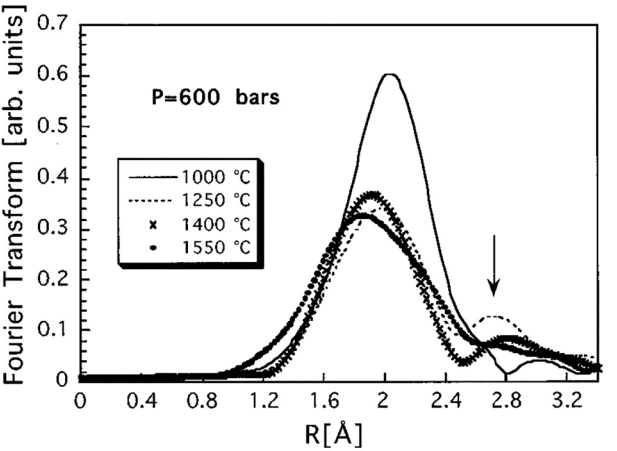

Figure 3: Modulus of Fourier transforms (FT) of the EXAFS signals for l-Se at 600 bar and various temperatures. A k^2 weighting factor and a Kaiser window ($\tau = 2.5$) have been used to calculate the FT. Reprinted with permission from [60].

[60]. The covalent bond length is greatly reduced to 2.22 Å in the metallic region from 2.33 Å in the semiconducting phase. This stronger bond is related to metallic conduction. The value of the shrinkage is more than twice that of the isolated Se chains against t-Se, suggesting the change of the conformation of the Se molecules, such as from helical to planar chains, where LP orbitals may form a strong covalent bond with overlapping each other. The appearance of a new bond around 2.9 Å in the metallic phase may be associated with interchain interactions and a network.

2.2 Liquid tellurium

While l-Se becomes metallic at high temperature near the critical point, l-Te shows metallic behavior even at the melting point. The structure of l-Te had been controversial, that is, the As-like threefold coordinated network structure [15], or the two-fold coordinated chain structure [16]. From the diffraction measurements with wide temperature range and/or wide range of a static structure factor the coordination number of the first neighbor is estimated to 2 [17–19, 63]. The details of the structure of the first neighbor were investigated by XAFS [20, 57, 58, 64, 66].

The Fourier transform of $\chi(k)$ for liquid Te including the supercooled state are shown in Figure 4 [20]. As the covalent bond of Se shrinks on melting, that of Te also shrinks, from 2.83 Å in t-Te to 2.79 Å in l-Te. In $|FT(r)|$, the second peak

assigned to the interchain atomic correlation sufficiently dampens compared with the first peak assigned to the covalent bond within the same chain. It implies that the interchain interaction is reduced, which induces the shrinkage of the covalent bond.

The analysis on the assumption that the pair distribution function $G(r)$ consists of one Gaussian curve gave about one for the coordination number of l-Te. The result is inconsistent with the neutron diffraction measurements [17–19], which show that the two-fold coordinated structure remains even in the liquid state. The analysis assumed two $G(r)$ gives the reliable results [20, 58]. Unlike l-Se, l-Te has two types of bonds, the long and short bonds. The lengths are 2.82 Å and 3.01 Å, just above the melting point, and the shorter bond length is a bit shorter than that of t-Se (2.84 Å). The fraction of the long bond is about half near the melting point. However, the fraction of the long bond reduces with decreasing temperature in a supercooled state, when l-Te transforms from a metallic to a semiconducting state. Therefore, the existence of the long bond relates to the metallic nature of l-Te.

2.3 Liquid mixture of Se-Te

Liquid Se-Te mixtures (l-Se-Te) are transformed from the semiconductor to metal by increasing the Te concentration and temperature following various physical properties for l-Se-Te mixtures, such as, density [27, 69], electrical conductivity [12, 25], and optical properties [7, 8, 24]. Therefore, information about the local structure of l-Se-Te provides important insight into the mechanism of the transition of liquid chalcogen. EXAFS is powerful tool to divide the interatomic correlation to Te-Te, Te-Se, Se-Te, Se-Se [57, 58, 65].

On melting, the covalent bond lengths for the nearest Se and Te atoms around the Te atoms $r_{\text{Te-Se}}$ and $r_{\text{Te-Te}}$ shorten from 2.59 to 2.53 Å, and from 2.83 to 2.75 Å, respectively [65]. The shrinkage is the same phenomenon that occurs with pure l-Se and l-Te. In the case of Se-Te mixtures, the interchain interactions affect the covalent bond length [58]. The Se-Se bond lengthens with an increasing Te concentration, which is brought about by the intra- and inter-chain transfer of LP electrons on the Te atom to an unoccupied antibonding orbital of the neighboring Se-Se bond. In an l-Se-Te mixture, there are also long and short Te-Te bonds, as with l-Te. With an increasing Te concentration or temperature, the fraction of the long Te-Te bond increases. The charge transfer between neighboring chains brings about electron delocalization around the Te atoms, inducing in the elongation of the Te-Te bonds. The fraction of Te around Se and Te shows a random distribution of Te on the Se-Te chains.

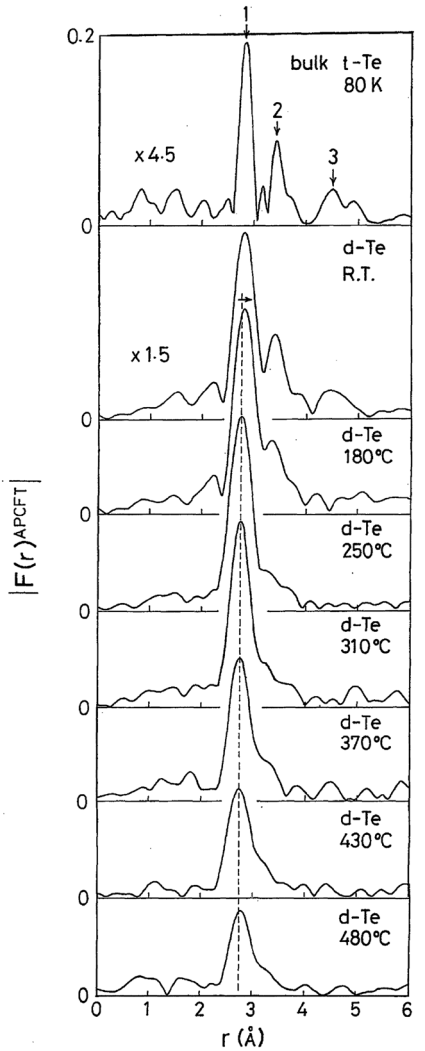

Figure 4: Magnitude of the amplitude- and phase-corrected Fourier transform of $\chi(k)$ for Te fine particles with a diameter of 20 nm confined in a NaCl matrix. Reproduced with permission from Ref. [20]. (c) (1995) The Physical Society of Japan.

2.4 Liquid mixtures of As-Te, As-Se, Ge-Se, and Ge-Te

In this subsection, we first discuss the XAFS studies for l-As-Te mixtures [67–71]. l-Te shows metallic character in the all temperature range higher than melting point. On the other hand, the liquid mixture of As-Te shows the SC-M transition at specific temperature range depending on the concentration and it is important to reveal the mechanism of the transitions for the origin of metallic feature.

As *K*-edge EXAFS for stoichiometric l-As_2Te_3 in the liquid state up to 900 °C has been studied [69]. An original sample cell made by polycrystalline sapphire was developed for the high temperature EXAFS measurements. A distinct EXAFS signal has been observed even at 900 °C. From the analysis of the EXAFS data, it is reported that the As-As atomic pairs exist in addition to As-Te in metallic l-As_2Te_3, whereas As and Te atoms are arranged as chemically ordered in crystalline As_2Te_3.

More wide concentration range for the l-As-Te mixture were surveyed by EXAFS, DC conductivity and Hall coefficient measurements [70]. The connection between the structures and the electronic properties for l-As_xTe_{100-x} mixtures ($18 < x < 40$) have been investigated. The EXAFS results indicate the presence of chemical disorder with the existence of As-As and Te-Te atomic pairs in l-As_xTe_{100-x} analogously to the previous study for the stoichiometric l-As_2Te_3. The network structure formed by threefold As atoms and two-fold Te atoms transforms to the two-fold chain structure around 500 °C.

On the other hand, it is interesting to consider the behavior at high temperature and As-rich region in l-As_xTe_{100-x}. Figure 5 shows the concentration variation of the coordination number, *N*, obtained from (a) As *K*-edge and Te *K*-edge EXAFS for l-As_xTe_{100-x} mixtures measured at 500 °C. The extrapolates of the plots for N_{As-Te} and N_{As-As} approach to about one and the sum of them, $N_{As(total)}$, is conserved around two up to 50 at.% As (in Figure 5 (a)). In Figure 5 (b), N_{Te-As} and N_{Te-Te}, and their sum, $N_{Te(total)}$, are also shown with the variation of As concentration. In this case N_{Te-As} increases to one but N_{Te-Te} decreases as increase of As concentration. Because of the large difference in bonding energies between As-Te (45 kcal mol^{-1}) and Te-Te (38 kcal mol^{-1}) bonds, the As atoms are favorite to make a covalent bond to Te atoms. This result indicates that a local atomic unit such as Te-As-As-Te exists at As rich region, in which both ends of -As-As- are connected by Te atoms. In other word, there are few Te-Te bond units, while As-As and As-Te much exist. The transformation from network to chain transformation occurs at higher temperature with higher As concentration. That is, the chains are very short at higher temperature and the Te atoms terminate the chain units.

The SC-M transition occurs by this network to chain transformation. These transitions could be demonstrated by the study of electric conductivity and Hall coefficient measurements. Let us discuss the microscopic viewpoint of the SC-M transition: The transition from the network to chain modifies the non-bonding and unfilled *p*-like electronic states. The dangling bonds located on Te atom produce the large fluctuations in the electric charge distribution, which results in an increase of the charge transfers. The increase of charge carriers and the production of new electron conduction path across the chains induce the SC-M transition.

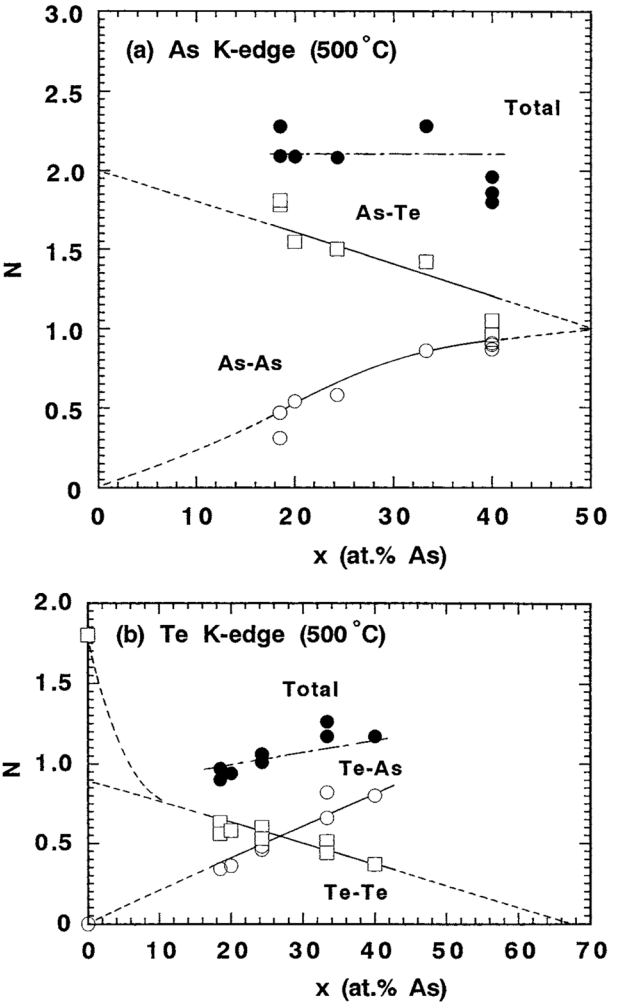

Figure 5: The coordination number, *N*, obtained from (a) As *K*-edge and (b) Te *K*-edge EXAFS as a function of the As composition for l-As_xTe_{100-x} mixtures measured at 500 °C. Open circles are N_{As-As} in (a) and N_{Te-As} in (b), open squares are N_{As-Te} in (a) and N_{Te-Te} in (b). Solid circles are the sum of N_{As-As} and N_{As-Te} in (a), and N_{Te-As} and N_{Te-Te} in (b). The lines are drawn as guides for the eye. Reprinted with permission from [70].

Next, we discuss the XAFS results for glassy (g-) and l-As_2Se_3 mixtures [35, 72–74]. EXAFS of the l- and g-As_2Se_3 were studied at the temperature range up to 500 °C [35]. EXAFS analysis indicates the existence of the chemical order but no As-As and Se-Se bonds in this temperature range. When the temperature decreases as

l-As_2Se_3 changes to the amorphous state, the interlayer correlation increases and the two-dimensional network structure transforms to a three-dimensional one. This transformation causes the change of the coordination number, N, at 300 °C, which is higher than T_g (181 °C).

The EXAFS investigations have been carried on l-As_2Se_3 over a wide temperature range under high pressure [74]. A formation of new As-As bonds in addition to the original As-Se bonds in the metallic region higher than 1000 °C are suggested by XAFS and X-ray scattering. Disappearance of the chemical order or the existence of the homopolar bonds induce the SC-M transition as previously discussed in l-As-Te mixture.

Liquid chalcogen and Ge mixture are also studied by XAFS [67, 69, 75]. Ge has four-fold covalent bonds and give an interesting effect onto threefold and two-fold chalcogen networks.

Se and Ge $K-$ edge for l-$GeSe_2$ were studied in the high temperature up to 1400 °C and under the pressure to 120 bar [67]. N around Se atom changes from two to one at 900 °C and the SC-M transition occurs. EXAFS spectra of Ge K-edge for l-$GeTe_2$ up to 1000 °C have been analyzed and the existence of the Ge-Ge bonds has been reported in metallic state of l-$GeTe_2$ [69].

Summarizing above discussions, the chemically disordered atomic pairs of chalcogen atoms and the collapse of the network structures induce the SC-M transition.

3 Amorphous chalcogens and chalcogenides

3.1 Amorphous state of Se-Te, Te, and Ge-Se

In this section, we discuss the structural studies for amorphous state of chalcogen mixtures by XAFS [76–95].

Se K-edge EXAFS study has been taken for a-Se-Te and the isolated Se-Te chains confined in the mordenite in comparison to the t-Se-Te [116]. The Se-Se and Se-Te bond distances in the Se-Te chain have been determined; the bond distance in the a-Se-Te shows the intermediate values between that for the isolated chains in the mordenite and that of t-Se-Te.

EXAFS of a-$Se_{1-x}Te_x$ ($0 < x < 0.4$) has been extensively studied on both of the Se and Te K-edges [80]. It was reported that the intrachain chemical order (existence of Se-Te atomic pairs) increases with Te content in the amorphous state. On the other hand, it was suggested that a random distribution of Se and Te atoms exists in the chains. And in the amorphous state, the thermal disorder dominates in the intrachain covalent bond.

The structure changes for Se under the amorphization process by a mechanical milling were studied [81]. t-Se has a chain structure by the combination between the strong intrachain covalent bonds and the weak interchain interactions as already discussed. It was reported that the interchain distance increases while the intrachain covalent bond distance decreases by the mechanical milling.

The local structure of the a-Te was investigated by EXAFS [87]. The a-Te film was obtained by deposition at liquid nitrogen temperature, and in-situ X-ray absorption was measured at the same temperature. The covalent bond distance decreases and the Debye-Waller factor of the intrachain decreases in a-Te in comparison with t-Te. The intrachain coordination number is around 2, which is almost same as t-Te, and the coordination number of the interchain interaction decreases. These results indicate that the primary intrachain structure remains in the amorphous state, but the secondary interchain interaction disappears. The strengthen of the intrachain interaction is enhanced by the decrease of the interchain interaction. Essentially the structure of amorphous state of chalcogens is similar to their liquid states.

Next, we discuss the amorphous state of Ge-contained chalcogenides. The XAFS results show the existence of the chemical ordering in the system [88]. EXAFS analysis shows that short-range order is fully preserved in the first shell throughout the present composition range. The coordination numbers of Ge and Se are unchanged.

The EXAFS studies on the structural change for a-$GeSe_2$, Ge_3Se_4 and Ge_4Se_5 prepared by mechanical milling have been carried out [91]. In $GeSe_2$ the short-range order remains during the milling process. The tetrahedral units in the crystalline rapidly decreases with increasing the milling time. Therefore, the amorphization is performed even at short milling time. On the other hand, it takes longer milling time for the amorphization of Ge_3Se_4 and Ge_4Se_5.

The structure of the amorphous and glassy state chalcogenides shows disordered arrangements and existence of homopolar atomic pairs in the systems as same as liquid state as discussed previously.

3.2 Photostructural change

In this subsection, we discuss the photostructural change inducing the photodarkening phenomenon of the amorphous chalcogenides, which is considered to be one of the most important applications, such as a photocopy, DVD-RAM and X-ray imaging sensors, etc. It is useful to survey the mechanism for the

photostructural change of the chalcogens and chalcogenides from the local structural point of view. [96–112].

EXAFS studies for reversible photostructural change have been carried out in the systems of $Ge_{33}Se_{67}$, $Ge_{40}Se_{60}$, $Ge_{40}S_{60}$, and $As_{40}S_{60}$, $As_{43}S_{57}$. In the As-S system, the photostructural change is characterized by an increase in the As-S-As bond angle (about 10°), whereas a mechanism of bond breaking and creation dominates in the Ge-S(Se) systems [99, 100].

The photostructural change in a-Se has been extensively studied by in-situ EXAFS by Kolobov et al. [101, 102, 105–107, 109]. The characteristics of the amorphous state are the strengthening of intrachain covalent bond and the weakening of interchain interactions. In a-Se, the coordination number is reported as 2.2 which means the presence of 20% threefold-coordinated sites. The increases of the average coordination number and structural disorder are observed under photostructural change, while the interatomic bond length remains.

Figure 6 shows a schematic diagram of the local structural change in a-Se as a result of the photoexitation. Interchain bond formation makes the threefold-coordinated sites by the photoexcitation. The formation of new bonds induces the increase of the coordination number of 1NN intrachain bond as shown in EXAFS. On the other hands, there are several pathways returning to the ground state as annealing. (path I, II, and III in the figure) These returning processes cause that the photostructural change is reversible.

Several mechanisms were proposed for the photostructural change process for each kind of chalcogenides. In any cases, the illumination of the light affects the electronic structures or the optical gaps and subsequently the combination of the networks and chains change.

4 Nanosized state

4.1 Nanoparticle of chalcogen

In this subsection, we discuss the structure of nanoparticles for Se and Te. As shown previously, Se and Te have hierarchic structures, and we discussed the primary and secondary interactions in the amorphous, liquid and confined state. From such point of view, the nanoparticles of chalcogens may show another interesting feature of the hierarchic structure.

EXAFS study has been carried out for Se nanoparticles with the sizes from 13 to 60 nm. Both the covalent bond distance and the nearest neighbor coordination number in the chain are unchanged while the interchain interaction weakens [113].

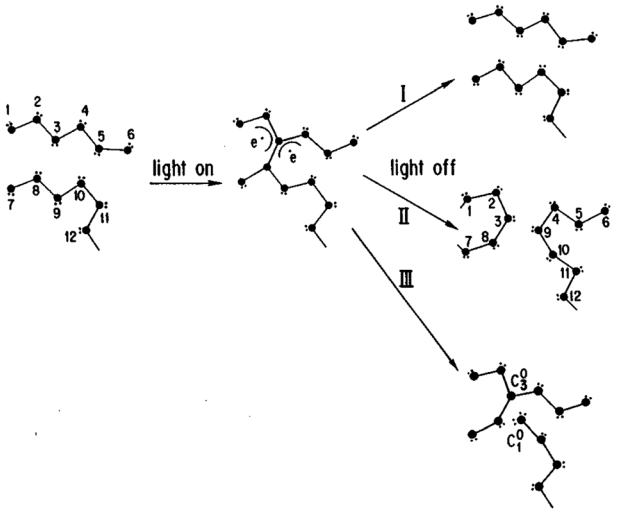

Figure 6: A schematic diagram of the local structural change in Se chains under the photostructural change. Reprinted with permission from [102].

While the change of intrachain structure in Se is quite small under the reduction of the particle size, Te nanoparticles show interesting features concerning to the relation of intrachain structure with interchain one. The interchain interaction is originated from the hybridization between the lone-pair orbitals and the anti-bonding orbitals in the adjacent chain.

The temperature dependent EXAFS study has been performed for t-Te and nanoparticle Te, which was made by island deposition with NaCl [114]. In the nanoparticle systems, the coordination number of the covalent bond is about 2. This means that two-fold coordinated chains, generally appears in t-Te, exist even in the Te nanoparticles. And further, the covalent bonds in the chain become stronger than those in t-Te, which is demonstrated by a shorter bond length and higher Einstein temperature obtained from temperature dependent EXAFS study.

Figure 7 shows the temperature dependence of σ^2 for the intrachain covalent bond. The solid lines are fitting by applying the correlated Einstein models for t-Te and the smaller particle size (0.5-nm-thick films). The static and the thermal contribution to σ^2, which is related to the Einstein temperature θ_E, are obtained from the model fitting. At all temperature range, the σ^2 of the smaller particle size are larger than that of t-Te and the larger particle size (300-nm-thick films). But the inclination of the σ^2 with temperature of the smaller particle is steeper than the larger particle size. The obtained value of θ_E of the smaller particle size is higher than the larger particle. This result indicates strengthening of covalent bond in the smaller Te nanoparticle.

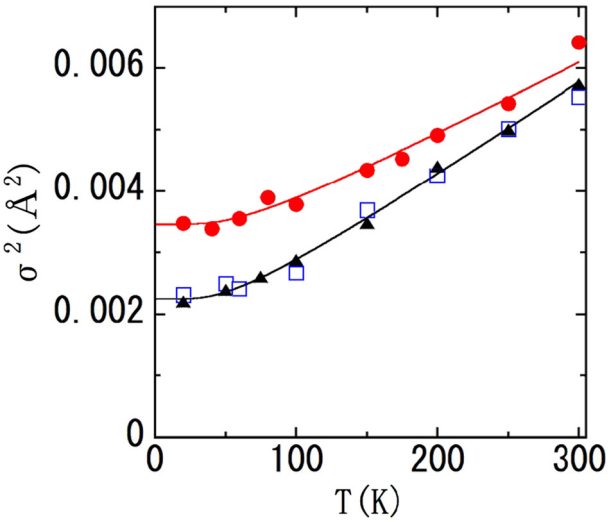

Figure 7: Temperature dependence of Debye-Waller factor σ^2 of the covalent bond in the chains. The correlated Einstein model was applied for t-Te and the 0.5-nm-thick films. The triangles are for t-Te, the squares are for the 300-nm-thick films, and the circles are for the 0.5-nm-thick films. Reprinted with permission from [114].

As previously discussed, weakening the interchain interaction induces the strengthen of intrachain covalent bond. The two-fold chain structure with covalent bond is preserve, the intrachain 1NN atomic distance (r_{intra}) shortens, and the interchain coordination number (N_{inter}) decreases with decreasing particle size. It is quite interesting that they have a strong correlation with each other [115]. The characteristic parameters for the discussion to the intra- and interchain interactions are r_{intra} and N_{inter}, respectively. In Figure 8 the r_{intra} is plotted with N_{inter}, which are obtained from the EXAFS for several film thicknesses. The smaller N_{inter} or the weaker interchain interaction, the stronger covalent bond in intrachain. r_{intra} reflects the force constant K_B of the covalent bond, and K_B has also correlation with N_{inter}. The weakening of the interchain interaction brings the strengthening of the covalent bond in the chain. The interchain secondary structure impacts the intrachain primary structure.

4.2 Confined chalcogen chains

Chalcogen atoms form chain/ring molecules as their primary structure, and bulk systems are formed by stacks of the molecules. It is important to understand the

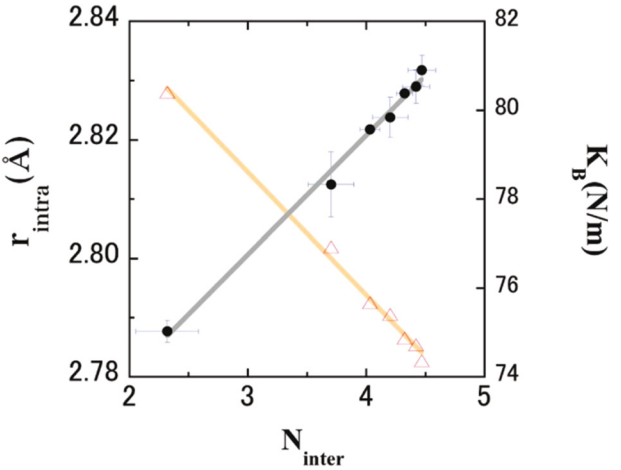

Figure 8: Correlation of the covalent bond length in the chain (r_{intra}) with the interchain coordination number (N_{inter}). That of the force constant (K_B) with N_{inter} is also shown. Black closed circles denote r_{intra}, red open triangles denote K_B. Straight lines are linear fits for each data. Reprinted with permission from [115].

primary structures as independent structures to understand chalcogen systems. Some materials have been chosen as host materials, which have a one-dimensional space where the chalcogen atoms can form a one-dimensional structure, such as mordenite, cancrinite and carbon nanotubes [45, 116–119].

Mordenite ($Na_2O{\cdot}Al_2O_3{\cdot}20SiO_2$) has one-dimensional channels with a 6.7 Å inner diameter [120]. In Se chains confined in mordenite [116], M–Se, the 1NN atomic distance locates at 2.33 Å, which is shorter than that of t-Se (2.37 Å) and close to that to a-Se (2.34 Å). The second nearest intrachain neighbor atomic distance is 3.61 Å, which is shorter than that of t-Se (3.72 Å) and a-Se (3.67 Å). These atomic distances imply that helical chains are formed in the mordenite and the covalent bond shrinks. The mechanism of shrinkage of the covalent bonds is the same for l-Se and M–Se, that is, the reduction of the interchain interaction brings about the shrinkage of the covalent bond. In chalcogen systems, the secondary structures are formed by the piling of elementary structures, and on the other hand the secondary structure affects the elementary structure. The mutual correlations are characteristic of chalcogen materials. Se-Te mixtures are confined in mordenite. The atomic distances $r_{Se\text{-}Se}$ from Se to Se, and $r_{Se\text{-}Te}$ from Se to Te in mordenite are shorter than those of t-Se-Te. It is interesting that $r_{Se\text{-}Se}$ elongates gradually as the Te concentration increases, while $r_{Se\text{-}Te}$ changes little. Se and Te atoms in mordenite, crystal, and amorphous form are randomly distributed.

The structure of single Se chains (Can-Se) confined in cancrinite ($Na_8Si_6Al_6O_{24}(OH)_2\,2H_2O$) was investigated using polarized XAFS [118]. The covalent bond length of Can-Se is 2.40 Å, which is longer than that of t-Se. The opposite result against M–Se, a-Se and l-Se is attributed to the interaction between Se atoms and the inner wall atoms of the cancrinite. Can-Se forms Se_2 dimers and is aligned along channels. They investigated other Se chains confined in mordenite and ALPO-5, and reported that Se chains form continuous helical chains and do not show strong polarization dependence.

5 Conclusion

We presented the reviews including the recent progresses for the structural study for the chalcogen elements and several chalcogenides in liquid, amorphous, and nanosized state by using XAFS. The chalcogen elements have hierarchic structures; the chain or ring structure constructed with the strong covalent bond as a primary structure, and the weaker interaction between chains as a secondary one. Existence of these two kinds of interactions induces exotic behaviors in these systems.

The liquid chalcogen elements and chalcogenide mixtures show the SC-M transition. For l-Se, the shrinkage of the chain with strengthen of the covalent bond is related to reduction of overlapping between LP orbital and antibonding orbital on adjacent chain, which induces the SC-M transition. In l-Te, shorter and longer covalent bonds appear in the chain. The long bond is considered to relate to the metallic nature. On the other hand, in l-As-Te mixture, As has a threefold coordination and the networks are formed in the SC region. When the network transforms to chain structure depending on the temperature and the components, the SC phase changes to metallic state. In case of Ge-chalcogen mixtures, the strong Ge-Ge bond relates to the SC-M transition.

Some of amorphous chalcogen elements and chalcogenides present photostructural change, which is the one of important industrial application. The change of optical property is related to the angle change of the covalent bond in a-As-S and the reversible transformation between chains and network structurers in a-Se. This behavior is also concerned with the relation between the primary covalent bond and the secondary interchain interaction.

From the study of nanosized state, the alternative role between the intra- and the interchain interactions is revealed, that is, the weakening the interchain interaction makes the intrachain covalent bond strong.

Acknowledgement: The authors are grateful to Professor H. Endo for suggesting the topic treated in this paper.

References

1. Cherin, P.; Unger, P. The crystal structure of trigonal selenium. *Inorg. Chem.* **1967**, *6*, 1589–1591.
2. Adenis, C.; Langer V; Lindqvist O. Reinvestigation of the structure of tellurium. *Acta Cryst.* **1989**, *C45*, 941–942.
3. Batsanov, S. S. Van der Waals Radii of Elements. *Inorg. Mater.* **2001**, *37*, 871–885.
4. Hoshino, H.; Schmutzler, R. W.; Hensel, F. The high temperature vapour pressure curve and the critical point of liquid selenium. *Ber. der Bunsengesellschaft fur phys. Chem.* **1976**, *80*, 27–31.
5. Hensel, F. Density-, temperature-, and concentration-induced metal-nonmetal transitions in fluids. *Can. J. Chem.* **1977**, *55*, 2225–2239.
6. Warren, W. W. , Jr.; Dupree, R. Structural and electronic transformations of liquid selenium at high temperature and pressure: A $_{77}$Se NMR study. *Phys. Rev. B* **1980**, *22*, 2257.
7. Seyer, H. P.; Tamura, K.; Hoshino, H.; Endo, H.; Hensel F. The optical properties of liquid Se and $Se_{1-x}Te_x$ alloys. *Ber. der Bunsengesellschaft fur phys. Chem.* **1986**, *90*, 587–592.
8. Ikemoto, H.; Yamamoto, I.; Yao, M.; Endo, H. The optical properties of liquid chalcogens at high temperature and pressure. *J. Phys. Soc. Jpn.* **1994**, *63*, 1611–1621.
9. Misawa, M.; Suzuki, K. Structure of chain molecule in liquid selenium by time-of-flight pulsed neutron diffraction. *Trans. Jap. Inst. Met.* **1977**, *18*, 427–434.
10. Edeling, M.; Freyland, W. Molecular Structure of Expanded Liquid Selenium up to 1400° C. *Ber. der Bunsengesellschaft fur phys. Chem.* **1981**, *85*, 1049–1054.
11. Tamura, K. Structural changes and the metal-non-metal transition insupercritical fluids. *J. Non-Cryst. Solids* **1996**, *205-207*, 239.
12. Perron, J. C. Electrical and thermoelectrical properties of selenium-tellurium liquid alloys. *Adv. Phys.* **1967**, *16*, 657–666.
13. Tourand, G.; Breuil, M. Etude par diffraction de neutrons de levolution en temperature de la structure du tellure liquide. *J. de Phys.* **1971**, *32*, 813.
14. Waseda, Y.; Tamaki, S. X-ray diffraction of molten Te and Tl-Te alloys. *Z. Naturforsch*. **1975**, *30a*, 1655.
15. Cabane, B.; Friedel, J. Local order in liquid tellurium. *J. de Phys.* **1971**, *32*, 73.
16. Cutler, M. *Liquid Semiconductors*; Academic Press: New York, **1977**.
17. Misawa, M. A short-chain model for local structure in liquid tellurium. *J. Phys.: Condens. Matter* **1992**, *4*, 9491–9500.
18. Menelle, A.; Bellissent, R.; Flank, A. M. Short range order in liquid Se-Te system by neutron scattering. *Phys. B* **1989**, *156-157*, 174–176.
19. Hoyer, W.; Neumann, H.; Wobst, N. Structure Investigation on Liquid Tellurium by X-Ray and Neutron Scattering. *Z. Naturforsch.* **1992**, *47a*, 833.
20. Tsuzuki, T.; Yao, M.; Endo, H. Static and dynamic structures of liquid Tellurium. *J. Phys. Soc. Jap.* **1995**, *64*, 485–503.
21. Tsuchiya, Y. Thermodynamic evidence for a structural transition of liquid Te in the supercooled region. *J. Phys.: Condens Matter* **1991**, *3*, 3163–3172.

22. Inui, M.; Noda, T.; Tamura, K.; Li, C. X-ray diffraction and small-angle x-ray scattering measurements on expanded fluid selenium. *J. Phys.: Condens. Matter* **1996**, *8*, 9347.
23. Hosokawa, S; Kuboi, T; Tamura, K. Density measurements for expanded fluid selenium up to the liquid-vapour supercritical region by the x-ray absorption method. *Ber. der Bunsen-Gesellschaft-Phys. Chem. Chem. Phys.* **1997**, *101*, 120–127.
24. Silva, L. A.; Cutler, M. Optical properties of liquid Se-Te alloys. *Phys. Rev. B* **1990**, *42*, 7103–7113.
25. Kao, S. S.; Cutler, M. Electronic behavior of selenium-rich selenium-tellurium liquid alloys. *Phys. Rev. B* **1988**, *38*, 9457.
26. Endo, H. Metal-nonmetal transitions in liquids under pressure. *J. Non-Cryst. Solids* **1984**, *61-62*, 1–12.
27. Thurn, H.; Ruska, J. Change of bonding system in liquid Se_xTe_{1-x} alloys as shown by density measurements. *J. Non-Cryst. Solids*. **1976**, *22*, 331–343.
28. Hoshino, H.i; Endo, H. Mass density of liquid selenium-tellurium mixtures at high temperatures and pressures. *J. Phys. Soc. Jap.* **1987**, *56*, 225–232.
29. Hosokawa, S; Yamada, S; Tamura, K. Density measurements for liquid Se-Te mixtures at high temperatures and pressures. *J. Non-Cryst. Solids* **1993**, *156-158*, 708–711.
30. Bellissent, R.; Tourand, G. Short range order in amorphous and liquid $Se_{1-x}Te_x$ systems. *J. Non-Cryst. Solids* **1980**, *35-36*, 1221–1226.
31. Hosokawa, S.; Sakaguchi, Y.; Hiasa, H.; Tamura, K. Optical absorption spectra of liquid As_2S_3 and As_2Se_3 over a wide temperature range *J. Phys.: Condens. Matter* **1991**, *3*, 6673–6677.
32. Ruska, J.; Thurn, H. Change of short-range order with temperature and composition in liquid Ge_xSe_{1-x} as shown by density measurements. *J. Non-Cryst. Solids* **1976**, *22*, 277–290.
33. Haisty, R.W.; Krebs, H. Electric conductivity of melts and their ability to form glasses: II. The Ge-As-Se system. *J. Non-Cryst. Solids* **1969**, *1*, 427.
34. Hosokawa, S.; Sakaguchi, Y.; Tamura, K. X-ray diffraction measurements for liquid As_2Se_3 up to the semiconductor-metal transition region. *J. Non-Cryst. Solids* **1992**, *150*, 35–39.
35. Hoshino, H.; Miyanaga, T.; Ikemoto, H.; Hosokoawa, S.; Endo, H. The semiconductor-metal transition of liquid arsenic-selenium mixtures at high temperatures and high pressures. *J. Non-Cryst. Solids* **1996**, *205*, 43–47.
36. Keneman, S. A. Hologram storage in arsenic trisulfide thin films. *Appl. Phys. Lett.* **1971**, *19*, 205.
37. Berkes, J. S.; S. W. Ing; W. J. Hillegas Photodecomposition of amorphous As_2Se_3 and As_2S_3. *J. Appl. Phys.* **1971**, *42*, 4908.
38. Pfeiffer, G.; Paesler, M.A. Identification of IRO structures in photodarkening: A high pressure study of As_2S_3 *J. Non-Cryst. Solids*. **1989**, *114*, 130.
39. Tanaka, K. Reversible photoinduced change in intermolecular distance in amorphous As_2S_3 network. *Appl. Phys. Lett.* **1975**, *26*, 243.
40. Nagels, P.; Sleeckx, E.; Callaerts, R.; L.Tichy Structural and optical properties of amorphous selenium prepared by plasma-enhanced CVD. *Solid State Commun.* **1995**, *94*, 49–52.
41. Ikemoto, H.; Tsuzuki, T.; Inui M.; Yao, M.; Endo H. Photodarkening of amorphous selenium under high pressure. *Z. fur Phys. Chem.* **2002**, *216*, 1107–1121.
42. Bogomolov, V.N.; Kholodkevich, S.V.; Romanov, S.G.; Agroskin, L.S. The absorption spectra of single selenium and tellurium chains in dielectric matrix channels. *Solid State Commun.* **1983**, *47*, 181–182.
43. Tamura, K.; Hosokawa, S.; Endo, H.; Yamasaki, S.; Oyanagi, H. The isolated se chains in the channels of mordenite crystal. *J. Phys. Soc. Jap.* **1986**, *55*, 528–533.

44. Endo, H.; Inui, M.; Yao, M.; Tamura, K.; Hoshino, H.; Katayama, Y.; Maruyama, K. Structure of isolated selenium chain in the channels of mordenite. *Z. Phys. Chem. Neue Folge* **1988**, *156*, 507–511.
45. Katayama, Y.; Maruyama, K.; Yao, M.; Endo, H. Spatial correlations and defects in isolated selenium-sulfur mixed chains. *J. Physi. Soc. Jap.* **1991**, *60*, 2229–2240.
46. Becker, J.; Rademann, K.; Hensel, F. Electronic and geometrical structure of Se_5, Se_6, Se_7, and Se_8. *Z. fur Naturforsch. A.* **1991**, *46a*, 453–461.
47. Yao, M.; Hayakawa, T.; Nagaya, K.; Ohmasa, Y.; Hamada, K.; Tai, M.; Yamamoto, I.; Nomura, M. X-ray absorption near edge structure of selenium free clusters. *Jap. J. Appl. Phys.* **1999**, *38*, 564.
48. Hayakawa, T.; Nagaya, K.; Hamada, K.; Ohmasa, Y.; Yao, M. Photoelectron photoion coincidence measurements of selenium cluster beam. II, Photon energy dependence. *J. Phys. Soc. Jpn.* **2000**, *69*, 2850–2858.
49. Yao, M.; Hayakawa, T.; Nagaya, K.; Hamada, K.; Ohmasa, Y.; Nomura, M. A new method for the size-selective EXAFS of neutral free clusters. *J. Synchrotron Radiat.* **2001**, *8*, 542–544.
50. Nagaya, K.; Yao, M.; Hayakawa, T.; Ohmasa, Y.; Kajihara, Y.; Ishii, M.; Katayama, Y. Size-selective extended X-ray absorption fine structure spectroscopy of free selenium clusters. *Phys. Rev. Lett.* **2002**, *89*, 243401.
51. Nagaya, K. EXAFS-PEPICO synchronous measurements for the size-selective structure analysis of neutral free clusters. *J. Phys. Soc. Jpn.* **2003**, *72*, 501–508.
52. Bunker, G. *Introduction to XAFS*. Cambridge University Press: Cambridge, **2010**.
53. Schnohr, C. S.; Ridgway, M. C. *X-ray absorption spectroscopy of semiconductors*. Springer: Heidelberg, **2015**.
54. Bunau, O.; Joly, Y. Self-consistent aspects of X-ray absorption calculations. *J. Phys.: Condens. Matter* **2009**, *21*, 345501.
55. Hatada, K.; Hayakawa, K.; Benfatto, M.; Natoli, C.R. Full-potential multiple scattering theory with space-filling cells for bound and continuum states. *J. Phys.: Condens. Matter* **2010**, *22*, 185501.
56. Miyanaga, T.; Fujikawa, T. XAFS spectroscopy: basic theory and recent developments. *J. Spectrosc. Dynam.* **2011**, *1*, 4.
57. Inui, M.; Tamura, K.; Yao, M.; Endo, H.; Hosokawa, S.; Hoshino, H. EXAFS studies on liquid Se-Te mixtures. *J. Non-Cryst. Solids* **1990**, *117-118*, 112–115.
58. Tamura, K.; Inui, M.; Yao, M.; Endo, H.;Hosokawa, S.; Hoshino, H.; Katyama, Y.; Maruyama, K. EXAFS measurements of liquid Se-Te mixtures. *J. Phy. Condens. Matter* **1991**, *3*, 7495–7510.
59. Hosokawa, S.; Tamura, K.; Inui, M.; Yao, M.; Endo, H.; Hoshino, H. Extended X-ray absorption fine-structure studies of dense selenium vapor. *J. Chem. Phy.* **1992**, *97*, 786–791.
60. Soldo, Y.; Hazemann, J. Semiconductor-to-metal transition in fluid selenium at high pressure and high temperature: an investigation using X-ray-absorption spectroscopy. *Phy. Rev. B* **1998**, *57*, 258–268.
61. Katayama, Y.; Tsuji, K.; Oyanagi, H.; Shimomura, O. Extended X-ray absorption fine structure study on liquid selenium under pressure. *J. Non-Cryst. Solids* **1998**, *232-234*, 93–98.
62. Inui, M.; Tamura, K.; Hazemann, J. L.; Raoux, D.; Soldo, Y.; Argoud, R.; Jal, J. F. X-ray absorption fine structure studies on expanded fluid Se: from liquid to dense vapor. *J. Non-Cryst. Solids*. **1999**, *250-252*, 525–530.
63. Enderby, J. E.; Barnes, A. C. Liquid semiconductors. *Rep. Prog. Phys.* **1990**, *53*, 85.
64. Endo, H. Structural and electronic-properties of liquid tellurium. *J. Non-Cryst. Solids*. **1993**, *156*, 700–702.

65. Miyanaga, T.; Crozier, E. D.; Seary, A. J.; Cutler, M.; Bell, F. G. Xafs study of sete in the liquid and solid states. *Jpn. J. Appl. Phys.* **1993**, *32*, 700–702.
66. Tsuzuki, T.; Sano, A.; Kawakita, Y.; Ohmasa, Y.; Yao, M.; Endo, H.; Inui, M.; Misawa, M. Structure of chalcogen nano-droplets. *J. Non-Cryst. Solids* **1993**, *156-15*, 695–699.
67. Tamura, K.; Hosokawa, S.; Sakaguti, Y.; Inui, M.; Endo, H. EXAFS measurements for liquid Ge-Se mixtures at high-temperatures and pressures. *Jpn. J. Appl. Phys.* **1993**, *32*, 694–695.
68. Tamura, K.; Hosokawa, S.; Inui, M.; Yao, M.; Endo, H.; Hoshino, H. EXAFS measurements for liquid As_2Se_3 at high temperatures and pressures. *J. Non-Cryst. Solids* **1992**, *150*, 351–355.
69. Hosokawa, S.; Tamura, K.; Inui, M.; Yao, M.; Endo, H.; Hoshino, H. EXAFS studies of liquid As_2Te_3 and $GeTe_2$. *J. Non-Cryst. Solids* **1993**, *156*, 712–715.
70. Endo, H.; Hoshino, H.; Ikemoto, H.; Miyanaga, T. Semiconductor-metal transition in liquid As-Te mixtures. *J. Phys. Condens. Matter* **2000**, *12*, 6077–6099.
71. Hoshino, H.; Endo, H.; Maruyama, K. The network-chain transformation in the liquid As-Te mixtures near the semiconductor-metal transition. *J. Res. Phys. Chem. Chem. Phyis.* **2003**, *217*, 847–861.
72. Hoshino, H.; Yamamoto, I.; Miyanaga, T;. Ikemoto, H; Endo, H. The electronic and structural changes in the supercooled liquid and glassy As_2Se_3. *J. Non-Cryst. Solids* **1999**, *250*, 478–482.
73. Ikemoto, H.; Hoshino, H.; Miyanaga, T.; Yamamoto, I.; Endo, H. The semiconductor-metal transition of liquid tellurium-arsenic mixtures. *J. Non-Cryst. Solids* **1999**, *250*, 458–462.
74. Hosokawa, S.; Tamura, K. Temperature driven semiconductor-metal transition and structural changes in liquid As_2Se_3. *J. Phys. Condens. Matter* **2004**, *16*, R1465–R1490.
75. Coulet, MV.; Testemale, D.; Hazemann, J-L.; Gaspard, J-P.; Bichara, C. Reverse Monte Carlo analysis of the local order in liquid $Ge_{0.15}Te_{0.85}$ alloys combining neutron scattering and X-ray absorption spectroscopy. *Phys. Rev. B* **2005**, *72*, 174209.
76. Federico, M.; Galli, G.; Magazu, S.; Majolino, D.; Burattini, E. Study of the glass-transition region in amorphous selenium by EXAFS. *Noovo Cimento*. **1988**, *10*, 425–434.
77. Ohmasa, Y.; Yamamoto, I.; Yao, M.; Endo, H. Structure and electronic properties of Te-Se mixtures under high pressure. *J. Phys. Soc. Jpn.* **1995**, *64*, 4766–4789.
78. Katayama, Y.; Kanda, H.; Tsuji, K.; Shimomura, O.; Oyanaga, H. EXAFS study of crystalline selenium under pressure. *Physica B* **1995**, *208*, 265–266.
79. Katayama, Y.; Tsuji, K.; Shimomura, O.; Oyanagi, H. EXAFS study of amorphous selenium under pressure. *J. Non-Cryst. Solids* **1996**, *205*, 199–202.
80. Majid, M.; Benazeth, S.; Souleau, C; Puran, J. XAFS study of interchain and intrachain order in $Se_{1-x}Te_x$ glasses: nearest neighbors. *Phys. Rev. B* **1998**, *58*, 6104–6114.
81. Zhao, YH.; Zhu, YT.; Liu, T. Mechanism of solid-state amorphization of Se induced by mechanical milling *J. Appl. Phys.* **2004**, *95*, 7674–7680.
82. Zhao, Y.; Zhu, Y.; Liu, T. EXAFS study of mechanical-milling-induced solid-state amorphization of Se. *J. Non-Cryst. Solids* **2004**, *333*, 246–251.
83. Machado, K. D.; Sanchez, D. F.; Maciel, G. A.; Brunatto, S. F.; Mangrich, A. S.; Stolf, S. F. Vibrational, optical and structural studies of an amorphous $Se_{0.90}S_{0.10}$ alloy produced by mechanical alloying. *J. Phys. Condens. Matter* **2009**, *21*, 195406.
84. Machado, K. D.; Dubiel, A. S.; Deflon, E.; Kostrzepa, I. M.; Stolf, S. F.; Sanchez, D. F.; Jovari, P. Investigation on vibrational and structural properties of amorphous $Se_{1-x}S_x$ alloys produced by mechanical alloying by Raman spectroscopy, X-ray diffraction EXAFS and RMC simulations. *Solid State Commun.* **2010**, *150*, 1359–1363.

85. Oliveira, E. C.; Deflon, E.; MacHado, K. D.; Silva, T. G.; Mangrich, A. S. Structural, vibrational and optical studies on an amorphous Se90P10 alloy produced by mechanical alloying. *J. Phys. Condens. Matter* **2012**, *24*, 115820.
86. Kostrzepa, I. M.; Siqueira, M. C.; MacHado, K. D.; MacIel, G. A.; Sanchez, D. F.; Brunatto, S. F. Structural investigations on an amorphous $Se_{90}Te_{10}$ alloy produced by mechanical alloying using EXAFS, cumulant expansion and RMC simulations. *J. Phys. Condens. Matter* **2012**, *24*, 125401.
87. Ikemoto, H.; Miyanaga, T. Local structure of amorphous tellurium studied by EXAFS. *J. Synchrotron Radiat.* **2014**, *21*, 409–412.
88. Zhou, W.; Paesler, M.; Sayers, D. Structure of germanium-selenium glasses- an X-ray absorption fine structure study. *Phys. Rev. B* **1991**, *43*, 2315–2321.
89. Lippens, PE; Brousse, E; Jumas, JC Local electronic structure of the tellurium atoms in As_2Te_3-GeTe compounds. *J. Phys. Chem. Solid.* **1999**, *60*, 1663–1668.
90. Wang, J. L.; Tsai, J. C.; Liu, C. T.; Nachimuthu, P.; Jang, L. Y.; Liu, R. G.; Chen, J. M. Structural properties of the glass system As-Se-S studied by x-ray absorption spectroscopy. *J. Appl. Phys.* **2000**, *88*, 2533–2540, PII [S0021-8979(00)09513-X].
91. Usuki, T; Araki, F; Uemura, O; kameda, Y.; Nasu, T.; Sakurai, M. Structure changes during amorphization of Ge-Se alloys by mechanical milling. *Mater. Trans.* **2003**, *44*, 344–350.
92. Golovchak, R.; Shpotyuk, O.; Kozdras, A.; Bureau, B.; Vlcek, M.; Ganjoo, A.; Jain, H. Atomistic model of physical ageing in Se-rich As-Se glasses. *Phil. Mag.* **2007**, *87*, 4323–4334.
93. Machado, K. D.; Sanchez, D. F.; Brunatto, S. F. Reverse Monte Carlo simulations of an amorphous Se-0 S-90(0) (10) alloy produced by mechanical alloying combining XRD and EXAFS data. *J. Non-Cryst. Solids* **2010**, *356*, 2865–2868.
94. Golovchak, R.; Kovalskiy, A.; Shpotyuk, O.; Jain, H. In search of energy landscape for network glasses *Appl. Phys. Lett.* **2011**, *98*, 171905.
95. MacHado, K. D.; Oliveira, E. C.; Deflon, E.; Stolf, S. F. EXAFS and cumulant expansion studies of an amorphous $Se_{90}P_{10}$ alloy produced by mechanical alloying. *Solid State Commun.* **2011**, *151*, 1280–1284.
96. Gladden, L; Elliott, S; Greaves, G; Cummings, S.; Rayment, T. EXAFS and neutron scattering studies of reversible photostructural change in bulk germanium chalcogenide glasses. *J. Non-Cryst. Solids* **1985**, *77-78*, 1199–1202.
97. Elliott, S. R.; Greaves, G. N.; Lowe, A. J.; Gladden, L. F.; Rennie, J. H. S. Studies of photostructural change in chalcogenide glasses. *J. phys.* **1986**, *47*, 363–368.
98. Yang, C.; Lee, J; Paesler, M.; Sayers, D. EXAFS Studies of thermostructural and photostructural chenges of vapor-depositted amorphous As_2S_3. *J. phys.* **1986**, *47*, 387–390.
99. Gladden, L.; Elliott, S.; Greaves, G. Photostructural change in bulk chalcogenide glasses: an EXAFS study. *J. Non-Cryst. Solids* **1988**, *106*, 189–192.
100. Elliott, S.; Kolobov, A. Photostructural change in amorphous $Se_{50}Se_{50}$ glasses. *Phil. mag.* **1990**, *61*, 853–858.
101. Kolobov, A.; Oyanagi, H.; Tanaka, K.; Tanaka, K. E. Photostructural changes in amorphous selenium: an in situ EXAFS study at low temperature. *J. Non-Cryst. Solids* **1996**, *198*, 709–713.
102. Kolobov, A.; Oyanagi, H.; Tanaka, K.; Tanaka, Ke. Structural study of amorphous selenium by in situ EXAFS: observation of photoinduced bond alternation. *Phys. Rev. B* **1997**, *55*, 726–734.
103. Kolobov, A.; Tanaka., K; Oyanagi, H. An EXAFS study of reversible photostructural changes in As_2Se_3 glass. *Phys. Solid State* **1997**, *39*, 64–67.

104. Kolobov, A; Oyanagi, H; Roy, A; Tanaka, K. A nanometer scale mechanism for the reversible photostructural change in amorphous chalcogenides. *J. Non-Cryst. Solids* **1998**, *232*, 80–85.
105. Oyanagi, H.; Kolobov, A.; Tanaka, K. Pump and probe X-ray absorption fine structure using high-brilliance photon sources. *J. Synchrotron Radiat.* **1998**, *5*, 1001–1003.
106. Kolobov, A.; Tanaka, K. Nanoscale mechanism of photoinduced metastability and reversible photodarkening in chalcogenide vitreous semiconductors. *Semiconductors* **1998**, *32*, 801–806.
107. Kolobov, A. V.; Oyanagi, H.; Kondo, M.; Matsuda, A.; Roy, A.; Tanaka, K. Photo-induced bond switching in amorphous chalcogenides. *J. Lumin.* **1999**, *83-84*, 205–208.
108. Chen, G.; Jain, H.; Khalid, S.; Li, J.; Drabold, D. A.; Elliott, S. R. Study of structural changes in amorphous As_2Se_3 by EXAFS under in situ laser irradiation. *Solid State Commun.* **2001**, *120*, 149–153.
109. Kolobov, A; Tominaga, J. Chalcogenide glasses in optical recording: recent progress. *J. Optoelectron. Adv. Mater.* **2002**, *4*, 679–686.
110. Chen, G.; Jain, H.; Khalid, S.; Li, J.; Drabold, D. A.; Elliott, S. R. Study of light-induced vector changes in the local atomic structure of As-Se glasses by EXAFS. *J. Non-Cryst. Solids* **2003**, *326*, 1257–262.
111. Ganjoo, A.; Chen, G.; Jain, H. Photoinduced changes in the local structure of a-$GeSe_2$ by in situ EXAFS. *Phys. Chem. Glasses* **2006**, *47*, 177–181.
112. Nemec, P.; Frumar, M. Photoinduced phenomena in As_4Se_3 amorphous thin films prepared by pulsed laser deposition. *Thin Sold Films* **2008**, *516*, 8377–8380.
113. Zhao, YH.; Lu, K.; Liu, T. EXAFS study of structural characteristics of nanocrystalline selenium with different grain sizes. *Phys. Rev. B* **1999**, *59*, 11117–11120.
114. Ikemoto, H.; Miyanaga, T. Extended X-ray absorption fine structure study of local structure and atomic correlations of tellurium nanoparticles. *Phys. Rev. Lett.* **2007**, *99*, 165503.
115. Ikemoto, H.; Goyo, A.; Miyanaga, T. Size dependence of the local structure and atomic correlations in tellurium nanoparticles. *J. Phys. Chem. C* **2011**, *115*, 2931–2937.
116. Inui, M.; Yao, M.; Endo, H. EXAFS study on selenium-tellurium mixed chains. *J. Phys. Soc. Jpn.* **1988**, *57*, 553–561.
117. Khouchaf, L.; Tuilier, M. H. Guth, J. L.; Elouadi, B. Atomic structure of selenium inserted in zeolites of the Na-mordenite type. *J. Phys. Chem. Solid* **1996**, *57*, 251–258.
118. Kolobov, A. V.; Oyanagi, H.; Poborchii, V. V.; Tanaka, K. Structure of single selenium chains confined in nanochannels of zeolites: a polarized X-ray absorption study. *J. Synchrotron Radiat.* **1999**, *6*, 362–363.
119. Chancolon, J.; Archaimbault, F.; Bonnamy, S.; Traverse, A.; Olivi, L.; Vlaic, G. Confinement of selenium inside carbon nanotubes, Structural characterization by X-ray diffraction and X-ray absorption spectroscopy. *J. Non-Cryst. Solids* **2006**, *352*, 99–108.
120. Hincapie, B. O.; Garces, L. J.; Zhang, Q.; Saccoc, A.; Suib, S. L. Synthesis of mordenite nanocrystals. *Microporous Mesoporous Mater.* **2004**, *67*, 19–26.